

Intrinsic ultralow lattice thermal conductivity of the unfilled skutterudite FeSb₃

Yuhao Fu,¹ David J. Singh,² Wu Li,^{3,*} and Lijun Zhang^{1,†}

¹College of Materials Science and Engineering and Key Laboratory of Automobile Materials of MOE, Jilin University, Changchun 130012, China

²Department of Physics and Astronomy, University of Missouri, Columbia, MO 65211-7010 USA

³Institute for Advanced Study, Shenzhen University, 3688 Nantian Avenue, Shenzhen 518060, China

(Dated: March 4, 2024)

It has been generally accepted that unfilled skutterudites possess high lattice thermal conductivity (κ_l) that can be efficiently reduced upon filling. Here by using first principles Boltzmann-Peierls transport calculations, we find pure skutterudite of FeSb₃ with no filler in fact has an intrinsic ultralow κ_l smaller than that of CoSb₃ by one order of magnitude. The value is even smaller than those of most of the fully filled skutterudites. This finding means that with FeSb₃ as a reference, filling does not necessarily lower κ_l . The ultralow κ_l of FeSb₃ is a consequence of much softened optical phonon branches associated with the weakly bonded Sb₄ rings. They overlap more with heat-carrying acoustic phonons and significantly increase the phase space for three-phonon anharmonic scattering processes. This provides an alternative non-filling related mechanism for lowering the κ_l of skutterudites.

Skutterudites are an important class of high performance thermoelectrics [1–20] as the embodiment of the Slack’s “electron-crystal phonon-glass” idea [21]. The existence of two isosahedron voids in their crystal structures allows for filling in a variety of cations (*e.g.*, rare earth, alkali earth or alkali metals). This offers dual advantages for good thermoelectrics: first, according to the Zintl concept the additional electrons transferred from the electropositive fillers to the CoSb₃ framework make possible flexible control of *n*-type doping [4, 7, 8, 10, 11, 15–17, 22, 23], and provides compensating change to the *p*-type doping with Co replaced by electron deficient Fe [1, 2, 5, 8, 14, 24]. Second, and more importantly, filling strongly lowers lattice thermal conductivity (κ_l) [1–4, 7, 8, 10, 11, 15, 17–19, 22] and optimizing the filling to lower κ_l both in terms of filling fraction and by using suitable mixtures of filled cations plays a central role in the optimization of high performance skutterudite thermoelectrics [4].

The physical mechanism responsible for the reduction of κ_l in filled skutterudites remains elusive after two decades of intensive research. There are several debated aspects about the nature and role of the vibrations associated with the filled “rattling” atoms: (i) whether the motion of the rattling atoms is incoherent and non-correlated [21, 25–27] or coherently couples with the host framework [28, 29]; (ii) whether there exists anharmonic interaction between the localized rattling modes and the propagating phonons of the host framework [30–34]; (iii) whether the reduction of κ_l originates from the energy dissipation caused by the resonant scattering of the rattling atoms [2, 21, 25, 35] or the enhanced conventional anharmonic (Umklapp) scattering processes [29, 33, 34, 36].

Despite controversy over the mechanism, there is consensus that the filling should reduce the κ_l of skutterudites. In this Letter we report the finding via first prin-

ciples transport calculations that the recently reported skutterudite FeSb₃ [37–42] often presumed to be closely related to CoSb₃ in fact has a very low κ_l without filling, even lower than those of most of the fully filled skutterudites (*e.g.*, with Ba, La and Ce). This ultralow κ_l in an unfilled skutterudite is a consequence of the much softened optical phonon branches that take the role of the rattling modes in the filled skutterudites. The emerged low-lying optical phonons overlap more with the heat-carrying acoustic phonons and increase three-phonon anharmonic scattering channels, thus significantly reducing phonon lifetimes and κ_l . This finding demonstrates an unexpected mechanism for the reduction of κ_l in skutterudites.

We perform first principles calculations of κ_l for FeSb₃ and fully filled skutterudites of La/CeFe₄Sb₁₂ by iteratively solving the linearized Boltzmann-Peierls transport equation of phonons with the SHENGBTE package [43] (see Supplementary methods for more details). The equilibrium crystal structures and interatomic force constants (IFCs) are obtained from DFT calculations with the plane-wave projector-augmented-wave method [44], as implemented in the VASP code [45]. We employ the local density approximation (LDA) as exchange-correlation functional. A ferromagnetic configuration for FeSb₃ is used, which is the lowest-energy magnetic configuration at the LDA level. Structural optimization is done with the kinetic energy cutoffs of 350 eV or more and the $8 \times 8 \times 8$ *k*-point mesh, which ensures the residual forces smaller than 1×10^{-4} eV/Å. The resulted equilibrium lattice constants are slightly smaller than the experimental data (by 2.03%, 1.78%, and 2.00% for FeSb₃, LaFe₄Sb₁₂ and CeFe₄Sb₁₂, respectively) as in Supplementary Table S1. The agreements are reasonably good by consideration of the usual underestimation of lattice constants in the DFT-LDA calculations. The harmonic and third-order anharmonic IFCs are calculated by using

the real-space supercell approach [43, 46], in a $3 \times 3 \times 3$ supercell with a $2 \times 2 \times 2$ k -point mesh and a $2 \times 2 \times 2$ supercell with a $3 \times 3 \times 3$ k -point mesh, respectively. The phonon momenta q -mesh of $15 \times 15 \times 15$ is used in solving the transport equation to ensure κ_l converged at the 1×10^{-6} W/mK level.

Fig. 1 shows calculated κ_l as the function of temperature for unfilled FeSb_3 and CoSb_3 [47], as well as fully filled skutterudites of $\text{LaFe}_4\text{Sb}_{12}$, $\text{CeFe}_4\text{Sb}_{12}$, $\text{YbFe}_4\text{Sb}_{12}$ [34], $\text{BaFe}_4\text{Sb}_{12}$ [34] and $\text{BaCo}_3\text{Sb}_{12}$ [33]. The excellent agreement between theoretical results of CoSb_3 and available experimental data [12, 48] strongly indicate the validity of our calculations. Surprisingly, we find that FeSb_3 exhibits a quite low κ_l of 1.14 W/mK at 300 K, about one order of magnitude lower than 11.6 W/mK of CoSb_3 . In the whole temperature range the κ_l of FeSb_3 is apparently much lower than the values of the most filled skutterudites (by more than two-third). The only exception is $\text{YbFe}_4\text{Sb}_{12}$ that owes the lowest theoretical κ_l among reported filled skutterudites [34].

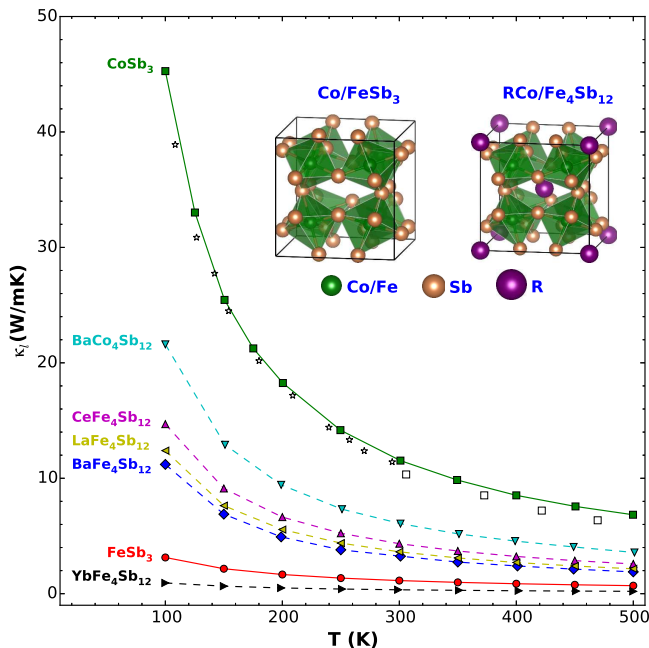


FIG. 1. (color online) Calculated temperature dependence of κ_l (in W/mK) of unfilled skutterudites (FeSb_3 , CoSb_3 [47]) and several fully filled skutterudites ($\text{LaFe}_4\text{Sb}_{12}$, $\text{CeFe}_4\text{Sb}_{12}$, $\text{YbFe}_4\text{Sb}_{12}$ [34], $\text{BaFe}_4\text{Sb}_{12}$ [34] and $\text{BaCo}_3\text{Sb}_{12}$ [33]). The experimental κ_l for CoSb_3 (open symbols) are taken from Morelli *et al.* (stars) [48] and Caillat *et al.* (squares) [12]. The inset shows crystal structures of unfilled and fully filled skutterudites.

We next elucidate the reason why FeSb_3 has such an ultralow κ_l . The physical factors that may affect κ_l (see Supplementary Eq. S1) include heat capacity C_λ , phonon velocity v_λ and phonon lifetime τ_λ of each phonon mode λ . Figs. 2a and 2b show the calculated

room-temperature heat capacity and the averaged group velocity over the long-wavelength acoustic phonons contributing predominately to heat-carrying, respectively. The difference in the heat capacities of FeSb_3 and CoSb_3 is negligibly small (less than 0.7%) and their values are $\sim 7\%$ lower than those of $\text{La/YbFe}_4\text{Sb}_{12}$. This is almost exactly as expected from the Dulong-Petit law, in accord with experiments (see Supplementary Fig. S1). The square of averaged phonon velocity for FeSb_3 is about 17% and 10% lower than that of CoSb_3 and $\text{LaFe}_4\text{Sb}_{12}$, respectively. This originates from the substantially reduced frequencies and velocities of the acoustic phonons in FeSb_3 (see below). However, the influences of these two factors are far from enough to explain the large discrepancies in κ_l . Therefore it must be the phonon lifetime that plays a central role in reducing κ_l of FeSb_3 .

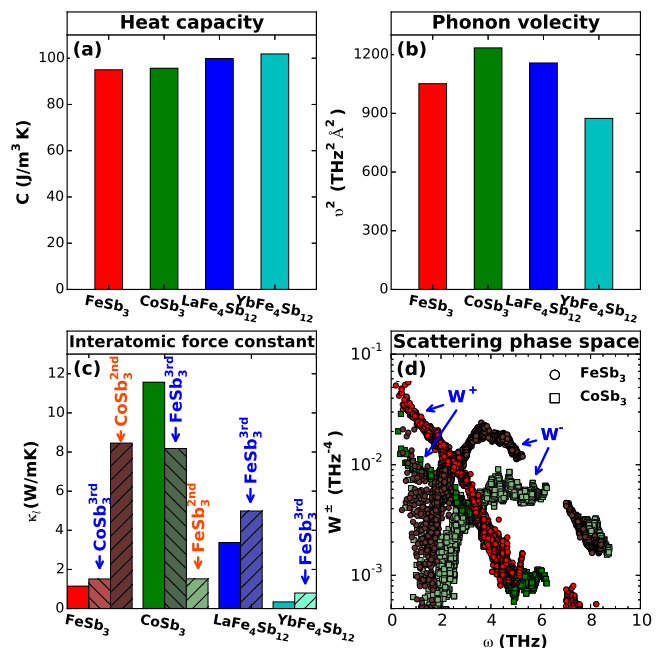


FIG. 2. (color online) Analysis of key factors that may affect κ_l for FeSb_3 , CoSb_3 and the filled skutterudites of $\text{La/YbFe}_4\text{Sb}_{12}$: (a) heat capacity, (b) phonon velocity, (c) interatomic force constant and (d) scattering phase space. In (b) the phonon velocity is calculated by averaging the group velocities of the long-wavelength (both transverse and longitudinal) acoustic phonons along different phonon momentum directions. In (c) the notation of M^{nth} represents that the n th-order IFCs of the compound M is used to replace the original IFCs when calculating the room-temperature κ_l .

The intrinsic phonon lifetimes of crystalline materials are primarily dominated by the three-phonon anharmonic scattering processes. Fig. 3 shows the calculated anharmonic scattering rates at 300 K. As seen, the scattering rates of FeSb_3 are nearly one order of magnitude larger than those of CoSb_3 in the low and intermediate frequency (ω) regions (below 5 THz). Clearly at

most of ω the rates of FeSb₃ are much higher than those of LaFe₄Sb₁₂, though lower than those of YbFe₄Sb₁₂. Therefore the observed differences in the anharmonic scattering processes that limit phonon lifetimes indeed account for the discrepancies in κ_l . Note that the anharmonic scattering rates of FeSb₃ are remarkably enhanced in a wide intermediate frequency range between ~ 1 and 5 THz. The behavior is similar to those in La/YbFe₄Sb₁₂ and other filled skutterudites [33, 34]. This affects contributions of phonon modes to κ_l , as indicated by the cumulative plot of κ_l (κ_l^c) that represents the fraction of heat carried by the phonons with less frequencies than ω (inset of Fig. 3). The higher anharmonic scattering rates correspond to the smaller lifetimes, and thus the less contributions of the phonons to κ_l . While for CoSb₃ κ_l^c increase rapidly with ω and the phonons below 2 THz have already contributed to $\sim 80\%$ of κ_l , κ_l^c of FeSb₃ show a much slower increase and the phonons below 2 THz only contribute to $\sim 50\%$ of κ_l . The behavior of κ_l^c of FeSb₃ resembles those of filled skutterudites, especially YbFe₄Sb₁₂.

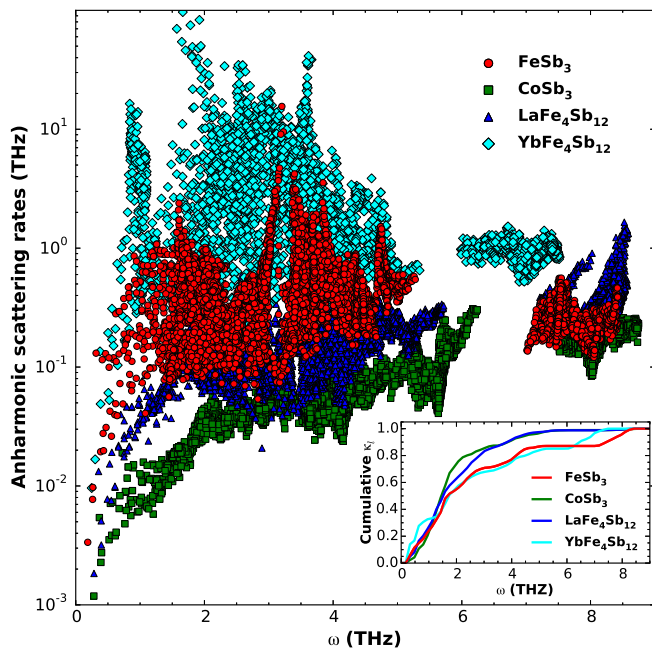


FIG. 3. (color online) Calculated anharmonic scattering rates of FeSb₃ (red circles), CoSb₃ (green squares), LaFe₄Sb₁₂ (blue triangles) and YbFe₄Sb₁₂ (cyan diamonds) at 300 K. The normalized cumulative κ_l as the function of ω is shown in the inset.

We further investigate the roles of harmonic and third-order anharmonic IFCs in enhancing three-phonon anharmonic scattering processes and reducing κ_l in FeSb₃. In particular we perform calculations of κ_l by deliberately interchanging the harmonic/anharmonic IFCs between two different compounds, as shown in Fig. 2c. For FeSb₃, when replacing the anharmonic IFCs by the ones from

CoSb₃ and remaining the other quantities unchanged, we find that κ_l increases by $\sim 30\%$, whereas κ_l of CoSb₃ decreases by $\sim 30\%$ when using the anharmonic IFCs from FeSb₃. The anharmonic scattering rates are generally proportional to the square of the anharmonic IFCs (Eq. S3 and S4). The result means the anharmonic IFCs of FeSb₃ are larger than those of CoSb₃, corresponding to the higher scattering rates in FeSb₃, but far from enough to account for its one-order lower κ_l . For the filled skutterudites of LaFe₄Sb₁₂ and YbFe₄Sb₁₂, when using the anharmonic IFCs from FeSb₃, the resulted κ_l show $\sim 50\%$ and $\sim 130\%$ increases, respectively. This indicates the anharmonic IFCs of FeSb₃ are smaller, corresponding to the lower scattering rates, which conflicts with the smaller κ_l of FeSb₃ than that of LaFe₄Sb₁₂. When we interchange the harmonic IFCs between FeSb₃ and CoSb₃, we find κ_l of FeSb₃ increases by about 8 times, and κ_l of CoSb₃ decreases by almost the same amount. The changes accord well with the discrepancy of κ_l between FeSb₃ and CoSb₃. From these results, we can conclude that the main factor responsible for the enhanced anharmonic scattering in FeSb₃ is the harmonic IFCs, rather than the third-order anharmonic IFCs.

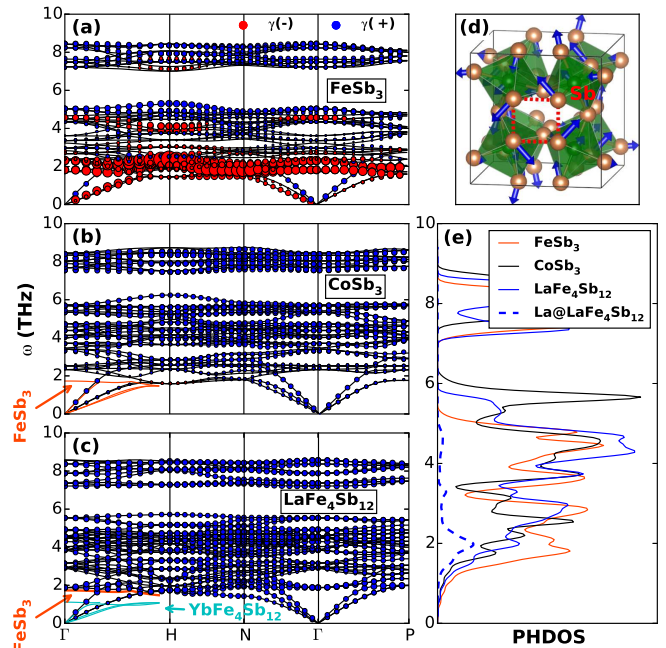


FIG. 4. (color online) (a,b,c) Calculated phonon dispersion curves of FeSb₃, CoSb₃ and LaFe₄Sb₁₂. The size of circle represents the magnitude of Grüneisen parameter (γ) for each mode, and the positive γ is shown in blue, negative in red. In (b) and (c) some phonon branches taken from FeSb₃ (in orange) and YbFe₄Sb₁₂ (in cyan) are shown for comparison. (d) Eigenvector of the lowest optical mode at the Γ point for FeSb₃. The Sb₄ ring is indicated with red dash lines. (e) shows the (projected) phonon density of states (PHDOS).

The specific way of the harmonic IFCs affecting the

anharmonic scattering processes is through phonon frequencies and eigenvectors (Eq. S3 and S4). The phonon eigenvectors contribute to the three-phonon scattering matrix elements. Usually for the same class of materials, the changes of eigenvectors with the varied harmonic IFCs are not as large as the changes of frequencies. It is thus reasonably to assume the scattering matrix elements do not change substantially here. The action of phonon frequencies on the anharmonic scattering is embodied by the three-phonon scattering phase space W^\pm (see Eq. S5), which depicts available three-phonon scattering channels among all modes. It consists of two components corresponding to absorption (W^+ , two phonons merging into one) and emission (W^- , one splitting into two) processes, respectively. As show in Fig. 2d, the W^+ of FeSb_3 are distinctly larger than those of CoSb_3 by several times in the low frequency (< 3.5 THz) region, and the W^- of FeSb_3 show much larger values in the wide frequency region below 5 THz as well. The origin of the significantly enhanced W^\pm of FeSb_3 lies in its distinct phonon spectrum. Comparing with that of CoSb_3 (Fig. 4b), the phonon spectrum of FeSb_3 (Fig. 4a) shows a clear softening for the lowest optical branch (down to below 2 THz). This optical branch is even lower in frequency than the La-derived rattling mode in $\text{LaFe}_4\text{Sb}_{12}$ (Fig. 4c), and is not far away from the extremely low frequency Yb-derived mode in $\text{YbFe}_4\text{Sb}_{12}$ (cyan curve in Fig. 4c). Actually it is not only the lowest optical branch, but several adjacent upper optical branches that become softened in FeSb_3 . This is unambiguously reflected by a sharp PHDOS peak appearing around 2 THz (Fig. 4e). It is located in the region similar to that of the La-derived rattling modes in $\text{LaFe}_4\text{Sb}_{12}$ (blue dash line in Fig. 4e). The low-lying optical phonons overlaps more with the acoustic branches, appreciably increases the phase space W^\pm for three-phonon scattering processes (Fig. 2d). This reduces significantly phonon lifetimes, which is the main root cause for the ultralow κ_l of FeSb_3 .

Fig. 4d shows the vibration pattern of the lowest optical phonon mode of FeSb_3 . It involves torsion of the Sb_4 ring, a typical quasi-molecular motif in skutterudites. The softening of this optical mode in FeSb_3 originates from the weaker Sb-Sb bonds of the Sb_4 ring, as demonstrated by the electron localization function contour plot in Fig. 5. Clearly the electrons in the Sb_4 ring of FeSb_3 are much less localized than the case of CoSb_3 . This indicates the rather weaker Sb-Sb bonds in FeSb_3 , as expected from its electron deficient nature. This is consistent with the fact that the Young modulus of FeSb_3 is smaller than that of CoSb_3 [40, 41]. As the result, the phonon modes that are mainly dominated by Sb atoms (below 6 THz) show general softening in FeSb_3 (Fig. 4e). The softening also occurs to the acoustic phonons, especially the transverse modes (Fig. 4b), which leads to the moderately reduced averaged phonon velocity of FeSb_3 in Fig. 2b. In addition to the phonon softening, the weaker

Sb-Sb bonds in FeSb_3 results in abnormal Grüneisen parameters (γ) of phonons (Fig. 4a). For the low-lying optical branches and the transverse acoustic phonons, the values of γ are negative (in red) and quite large in magnitude. Such phonon modes with the large magnitude γ in principle facilitate high lattice anharmonicity [49] and thus low κ_l . The negative sign of γ for the low-lying optical branches implies that they will be further softened under contraction. This is expected to cause the more overlapping with acoustic phonons, more enhanced W^\pm and thus even lower κ_l at high pressures.

For the filled skutterudites, the electrons of filler transfer to the host framework following the Zintl behavior. These electrons primarily distribute on the Sb_4 ring, which considerably strengthens the Sb-Sb covalent bonds, as indicated in Fig. 5c for the $\text{LaFe}_4\text{Sb}_{12}$ case. This is consistent with the band structure of skutterudites, which shows a light Sb derived band at the top of the valence bands [50]. This may also explain why filled Fe-based skutterudites are easier to form than FeSb_3 usually stabilized in films [37, 39, 40]. If one considers only the fact that the strengthened Sb-Sb bonds after La filling lift the Sb-derived optical branches in $\text{LaFe}_4\text{Sb}_{12}$, an increase of κ_l is expected. In fact, the La filler derived rattling modes take the role to remarkably enhance W^\pm . As the result κ_l of $\text{LaFe}_4\text{Sb}_{12}$ is still much lower than that of CoSb_3 , and only about three times larger than that of FeSb_3 . For the case of $\text{YbFe}_4\text{Sb}_{12}$, the Yb derived even lower frequency and rather flat optical phonon branches increase W^\pm more significantly, resulting in the more reduced κ_l [34].

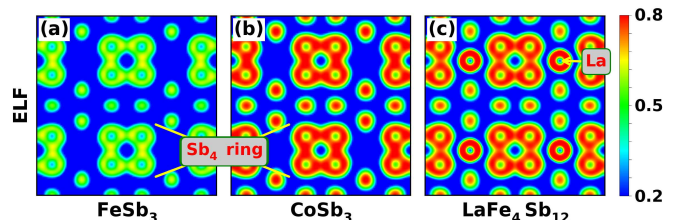


FIG. 5. (color online) Contour plot of electron localization function within the (100) plane of (a) FeSb_3 , (b) CoSb_3 and (c) $\text{LaFe}_4\text{Sb}_{12}$.

To summarize, we report a discovery of ultralow lattice thermal conductivity (κ_l) of pure skutterudite FeSb_3 with no filler by using first principles Boltzmann-Peierls transport simulations. The calculated κ_l is only 1.14 W/mK at room temperature, one order of magnitude lower than that of CoSb_3 . It is even lower than the values of the most fully filled skutterudites. This is in contrast to the generally accepted approach where filling is used for reduction of κ_l in skutterudites. The origin of the ultralow κ_l is attributed to the remarkably softened optical phonon branches associated with the weaker Sb-Sb bonds in FeSb_3 owing to its electron deficient nature. These low

frequency optical phonons, having similar frequencies to those of the rattling modes in filled skutterudites, take the role of the rattling modes. They overlap more with the heat-carrying acoustic phonons and increase significantly the phase space of three-phonon anharmonic scattering processes. This leads to much reduced phonon lifetimes, and thus very low intrinsic κ_l . By finding the intrinsic ultralow κ_l of an unfilled skutterudite, our results offer new insight into the still debated mechanism responsible for the reduction of κ_l upon filling in skutterudites. Finally we evaluate the maximum mean free path of phonons for bulk FeSb₃ and find the value smaller than 600 nm (Supplementary Fig. S3), suggesting that the experimentally synthesized FeSb₃ films [40] can be directly applied to verify our theoretical prediction.

The authors acknowledge funding support from the Recruitment Program of Global Youth Experts in China and special funds for talent development in Jilin Province. Part of calculations was performed in the high performance computing center of Jilin University. Work of D.J.S. is supported by S3TEC an Energy Frontier Research Center funded by the Department of Energy, Office of Science, Basic Energy Sciences under award #DE-SC0001299 / DE-FG02-09ER46577.

* wu.li.phys2011@gmail.com

† lijun_zhang@jlu.edu.cn

- [1] D. T. Morelli and G. P. Meisner, *J. Appl. Phys.* **77**, 3777 (1995).
- [2] B. C. Sales, D. Mandrus, and R. K. Williams, *Science* **272**, 1325 (1996).
- [3] G. S. Nolas, D. T. Morelli, and T. M. Tritt, *Annu. Rev. Mater. Sci.* **29**, 89 (1999).
- [4] X. Shi, J. Yang, J. R. Salvador, M. Chi, J. Y. Cho, H. Wang, S. Bai, J. Yang, W. Zhang, and L. Chen, *J. Am. Chem. Soc.* **133**, 7837 (2011).
- [5] D. J. Singh and I. I. Mazin, *Phys. Rev. B* **56**, R1650 (1997).
- [6] W. Zhang, X. Shi, Z. G. Mei, Y. Xu, L. D. Chen, J. Yang, and G. P. Meisner, *Appl. Phys. Lett.* **89**, 112105 (2006).
- [7] D. T. Morelli, G. P. Meisner, B. Chen, S. Hu, and C. Uher, *Phys. Rev. B* **56**, 7376 (1997).
- [8] G. Rogl, A. Grytsiv, E. Bauer, P. Rogl, and M. Zehetbauer, *Intermetallics* **18**, 57 (2010).
- [9] W. Schnelle, A. Leithe-Jasper, H. Rosner, R. Cardoso-Gil, R. Gumeniuk, D. Trots, J. A. Mydosh, and Y. Grin, *Phys. Rev. B* **77**, 094421 (2008).
- [10] H. Li, X. Tang, Q. Zhang, and C. Uher, *Appl. Phys. Lett.* **94**, 102114 (2009).
- [11] J. S. Dyck, W. Chen, C. Uher, L. Chen, X. Tang, and T. Hirai, *J. Appl. Phys.* **91**, 3698 (2002).
- [12] T. Caillat, A. Borshchevsky, and J. Fleurial, *J. Appl. Phys.* **80**, 4442 (1996).
- [13] J. Yang and T. Caillat, *MRS Bull.* **31**, 224 (2006).
- [14] J. Yang, P. Qiu, R. Liu, L. Xi, S. Zheng, W. Zhang, L. Chen, D. J. Singh, and J. Yang, *Phys. Rev. B* **84**, 235205 (2011).
- [15] G. S. Nolas, M. Kaeser, R. T. Littleton, and T. M. Tritt, *Appl. Phys. Lett.* **77**, 1855 (2000).
- [16] L. D. Chen, T. Kawahara, X. F. Tang, T. Goto, T. Hirai, J. S. Dyck, W. Chen, and C. Uher, *J. Appl. Phys.* **90**, 1864 (2001).
- [17] G. A. Lamberton, S. Bhattacharya, R. T. Littleton, M. A. Kaeser, R. H. Tedstrom, T. M. Tritt, J. Yang, and G. S. Nolas, *Appl. Phys. Lett.* **80**, 598 (2002).
- [18] L. Zhang, A. Grytsiv, P. Rogl, E. Bauer, and M. Zehetbauer, *J. Phys. D: Appl. Phys.* **42**, 225405 (2009).
- [19] G. Rogl, A. Grytsiv, P. Rogl, N. Peranio, E. Bauer, M. Zehetbauer, and O. Eibl, *Acta Mater.* **63**, 30 (2014).
- [20] J. Yang, L. Xi, W. Qiu, L. Wu, X. Shi, L. Chen, J. Yang, W. Zhang, C. Uher, and D. J. Singh, *npj Comput. Mater.* **2**, 15015 (2016).
- [21] G. A. Slack, in *CRC Handbook of Thermoelectrics*, edited by D. M. Rowe (CRC Press, Boca Raton, FL, 1995) pp. 402–406.
- [22] X. Y. Zhao, X. Shi, L. D. Chen, W. Q. Zhang, W. B. Zhang, and Y. Z. Pei, *J. Appl. Phys.* **99**, 053711 (2006).
- [23] Y. Z. Pei, L. D. Chen, W. Zhang, X. Shi, S. Q. Bai, X. Y. Zhao, Z. G. Mei, and X. Y. Li, *Appl. Phys. Lett.* **89**, 221107 (2006).
- [24] P. F. Qiu, J. Yang, R. H. Liu, X. Shi, X. Y. Huang, G. J. Snyder, W. Zhang, and L. D. Chen, *J. Appl. Phys.* **109**, 063713 (2011).
- [25] G. A. Slack and V. G. Tsoukala, *J. Appl. Phys.* **76**, 1665 (1994).
- [26] V. Keppens, D. Mandrus, B. Sales, B. Chakoumakos, P. Dai, R. Coldea, M. Maple, D. Gajewski, E. Freeman, and S. Bennington, *Nature* **395**, 876 (1998).
- [27] R. P. Hermann, R. Jin, W. Schweika, F. Grandjean, D. Mandrus, B. C. Sales, and G. J. Long, *Phys. Rev. Lett.* **90**, 135505 (2003).
- [28] H.-C. Wille, R. P. Hermann, I. Sergueev, O. Leupold, P. van der Linden, B. C. Sales, F. Grandjean, G. J. Long, R. Rüffer, and Y. V. Shvyd'ko, *Phys. Rev. B* **76**, 140301 (2007).
- [29] M. M. Koza, M. R. Johnson, R. Viennois, H. Mutka, L. Girard, and D. Ravot, *Nat. Mater.* **7**, 805 (2008).
- [30] J. L. Feldman, D. J. Singh, I. I. Mazin, D. Mandrus, and B. C. Sales, *Phys. Rev. B* **61**, R9209 (2000).
- [31] A. Yamakage and Y. Kuramoto, *J. Phys. Soc. Jpn.* **78**, 064602 (2009).
- [32] N. Bernstein, J. L. Feldman, and D. J. Singh, *Phys. Rev. B* **81**, 134301 (2010).
- [33] W. Li and N. Mingo, *Phys. Rev. B* **89**, 184304 (2014).
- [34] W. Li and N. Mingo, *Phys. Rev. B* **91**, 144304 (2015).
- [35] B. C. Sales, D. Mandrus, B. C. Chakoumakos, V. Keppens, and J. R. Thompson, *Phys. Rev. B* **56**, 15081 (1997).
- [36] C. H. Lee, I. Hase, H. Sugawara, H. Yoshizawa, and H. Sato, *J. Phys. Soc. Jpn.* **75**, 123602 (2006).
- [37] M. V. Daniel, L. Hammerschmidt, C. Schmidt, F. Timmermann, J. Franke, N. Jöhrmann, M. Hietschold, D. C. Johnson, B. Paulus, and M. Albrecht, *Phys. Rev. B* **91**, 085410 (2015).
- [38] G. Xing, X. Fan, W. Zheng, Y. Ma, H. Shi, and D. J. Singh, *Sci. Rep.* **5** (2015).
- [39] M. D. Hornbostel, E. J. Hyer, J. Thiel, and D. C. Johnson, *J. Am. Chem. Soc.* **119**, 2665 (1997).
- [40] A. Möchel, I. Sergueev, N. Nguyen, G. J. Long, F. Grandjean, D. C. Johnson, and R. P. Hermann, *Phys. Rev. B* **84**, 064302 (2011).

- [41] M. Råsander, L. Bergqvist, and A. Delin, Phys. Rev. B **91**, 014303 (2015).
- [42] S. Lemal, N. Nguyen, J. de Boor, P. Ghosez, J. Varignon, B. Klobes, R. P. Hermann, and M. J. Verstraete, Phys. Rev. B **92**, 205204 (2015).
- [43] W. Li, J. Carrete, N. A. Katcho, and N. Mingo, Comput. Phys. **185**, 1747 (2014).
- [44] P. E. Blöchl, Phys. Rev. B **50**, 17953 (1994).
- [45] G. Kresse and J. Furthmüller, Phys. Rev. B **54**, 11169 (1996).
- [46] A. Togo, F. Oba, and I. Tanaka, Phys. rev. B **78**, 134106 (2008).
- [47] W. Li and N. Mingo, Phys. Rev. B **90**, 094302 (2014).
- [48] D. T. Morelli, T. Caillat, J.-P. Fleurial, A. Borshchevsky, J. Vandersande, B. Chen, and C. Uher, Phys. Rev. B **51**, 9622 (1995).
- [49] J. S. Dugdale and D. K. C. MacDonald, Phys. Rev. **98**, 1751 (1955).
- [50] D. J. Singh and W. E. Pickett, Phys. Rev. B **50**, 11235 (1994).

Supplemental Material for “Intrinsic ultralow lattice thermal conductivity of the unfilled skutterudite FeSb₃”

Yuhao Fu,¹ David J. Singh,² Wu Li,³ and Lijun Zhang¹

¹*College of Materials Science and Engineering and Key Laboratory of Automobile Materials of MOE, Jilin University, Changchun 130012, China*

²*Department of Physics and Astronomy, University of Missouri, Columbia, MO 65211-7010 USA*

³*Institute for Advanced Study, Shenzhen University, 3688 Nanhai Avenue, Shenzhen 518060, China*

(Dated: March 4, 2024)

SUPPLEMENTARY MEDTHODS

The first principles calculations of lattice thermal conductivity (κ_l) are performed by solving the linearized Boltzmann-Peierls transport equation of phonons [1]. All the contributions from two-phonon and three-phonon scattering processes responsible for intrinsic κ_l of crystalline materials are included. Briefly the isotopic κ_l of cubic skutterudites at temperature T can be represented as the sum of contributions over each phonon mode λ (with branch p and wave vector \mathbf{q}):

$$\kappa_l \equiv \kappa_l^{\alpha\alpha} = \frac{1}{NV} \sum_{\lambda} C_{\lambda} v_{\lambda}^{\alpha} v_{\lambda}^{\alpha} \tau_{\lambda}, \quad (\text{S1})$$

and

$$C_{\lambda} = \frac{\partial f_{\lambda}(\omega_{\lambda}, T)}{\partial T}, \quad (\text{S2})$$

where N is the number of \mathbf{q} points uniformly sampled in the phonon Brillouin zone, V is the unit cell volume, C_{λ} is the phonon mode heat capacity, $f_{\lambda}(\omega_{\lambda}, T)$ is the Bose-Einstein distribution form that is the function of the phonon frequency ω_{λ} and T, v_{λ}^{α} is the phonon group velocity along the α direction, and τ_{λ} is the phonon lifetime. In bulk materials without impurities, τ_{λ} is determined by the processes of two-phonon scattering from isotopic disorder and three-phonon anharmonic scattering. In the relaxation time approximation, τ_{λ} is equal to a sum of the isotope scattering rate ($\frac{1}{\tau_{iso}}$) and the anharmonic scattering rate ($\frac{1}{\tau_{anh}}$). For most of materials, $\frac{1}{\tau_{iso}}$ is at least two-order smaller in magnitude than $\frac{1}{\tau_{anh}}$. $\frac{1}{\tau_{anh}}$ can be calculated as the sum over λ of the three-phonon transition probabilities $\Gamma_{\lambda\lambda'\lambda''}^{\pm}$, which can be expressed as [1-4]:

$$\Gamma_{\lambda\lambda'\lambda''}^{\pm} = \frac{\hbar\pi}{8N} \left\{ \frac{2(f_{\lambda'} - f_{\lambda''})}{f_{\lambda'} + f_{\lambda''} + 1} \right\} \frac{\delta(\omega_{\lambda} \pm \omega_{\lambda'} - \omega_{\lambda''})}{\omega_{\lambda}\omega_{\lambda'}\omega_{\lambda''}} |V_{\lambda\lambda'\lambda''}^{\pm}|^2, \quad (\text{S3})$$

and

$$V_{\lambda\lambda'\lambda''}^{\pm} = \sum_{i \in u.c.} \sum_{j,k} \sum_{\alpha\beta\gamma} \frac{e_{\lambda}^{\alpha}(i) e_{p', \pm q'}^{\beta}(j) e_{p'', -q''}^{\gamma}(k)}{\sqrt{M_i M_j M_k}} \Phi_{ijk}^{\alpha\beta\gamma}, \quad (\text{S4})$$

where the upper (lower) row in curly brackets corresponds to the +(-) sign of $\Gamma_{\lambda\lambda'\lambda''}^{\pm}$, which represent three-phonon absorption (two phonons merging into one phonon) and emission (one phonon splitting into two) processes. The scattering matrix elements $V_{\lambda\lambda'\lambda''}^{\pm}$ can be evaluated with the normalized eigenvectors $e_{p,q}$ of the three phonons involved and the anharmonic interatomic force constants (IFCs) $\Phi_{ijk}^{\alpha\beta\gamma}$ [1, 4]. The contribution of harmonic phonon frequencies to the anharmonic scattering rates can be represented by the three-phonon scattering phase space W^{\pm} (+ and - signs corresponding to absorption and emission processes). It is defined as the sum of frequency-containing factors in the expression of three-phonon transition probabilities (Eq. S3), and is written as [5]:

$$W_{\lambda}^{\pm} = \frac{1}{2N} \sum_{\lambda' p''} \left\{ \frac{2(f_{\lambda'} - f_{\lambda''})}{f_{\lambda'} + f_{\lambda''} + 1} \right\} \frac{\delta(\omega_{\lambda} \pm \omega_{\lambda'} - \omega_{\lambda''})}{\omega_{\lambda}\omega_{\lambda'}\omega_{\lambda''}}. \quad (\text{S5})$$

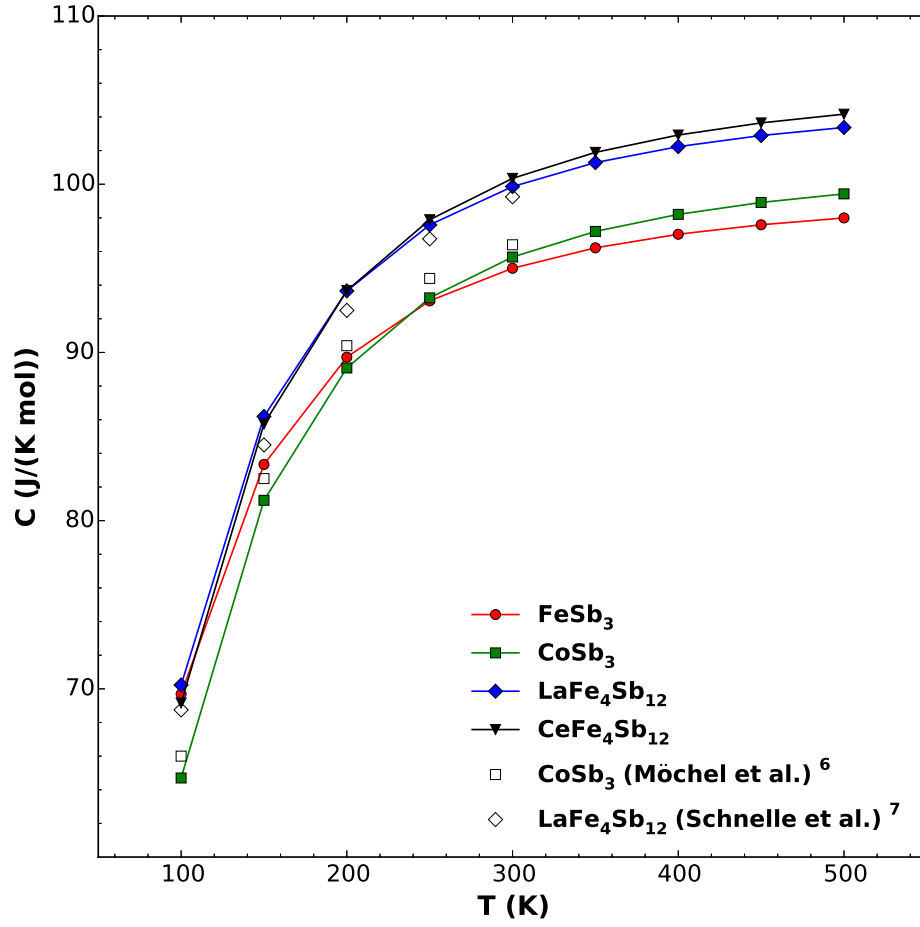


FIG. S1. (color online) Calculated heat capacity as the function of temperature for FeSb₃, CoSb₃, LaFe₄Sb₁₂ and CeFe₄Sb₁₂. The available experimental data for CoSb₃ [6] and LaFe₄Sb₁₂ [7] are shown for comparison. The agreement between our calculation and the experiments is good. **In addition to this comparison, the validity of our first principles calculations is also indicated by the comparison of κ_l for CoSb₃ between our theory and available experiments in Fig. 1 of the main text, as well as the following comparison of phonon spectrum for LaFe₄Sb₁₂ (Fig. S2).**

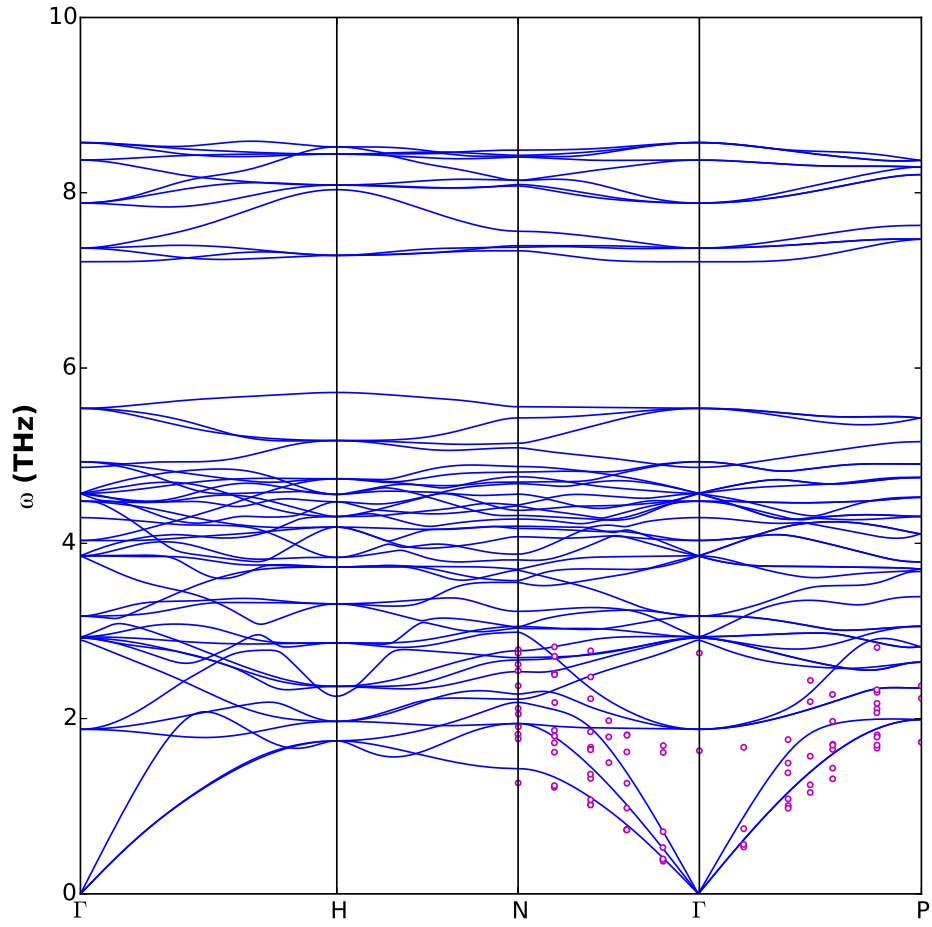


FIG. S2. (color online) Calculated phonon dispersion curves of LaFe₄Sb₁₂. The available experimental data from inelastic neutron scattering measurements [8] are shown for comparison. The agreement between our calculation and the experiment is reasonably good.

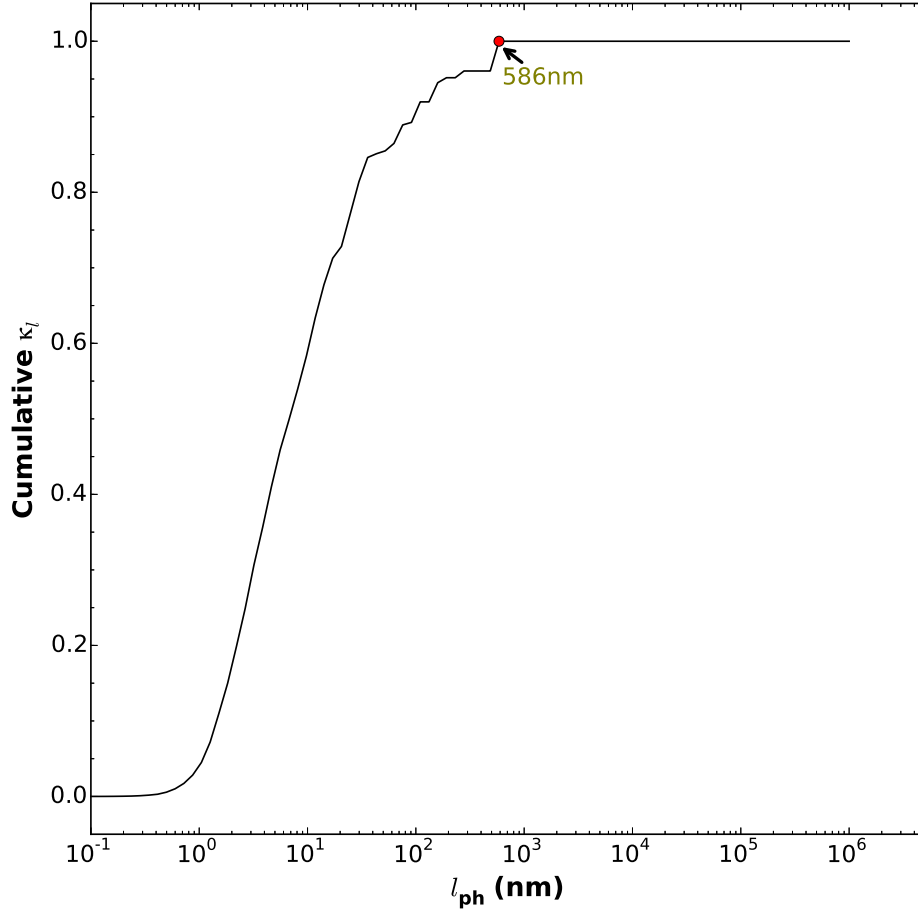


FIG. S3. (color online) The normalized cumulative κ_l of FeSb₃ as a function of the phonon mean free path (l_{ph}) at 300 K. The maximum l_{ph} among all the modes, which corresponds to the onset point of the cumulative κ_l becoming constant (equal to 1.0), is indicated. **The purpose of this calculation is to provide a reference to future experimental measurements for how thick thin-film samples are required to take on the intrinsic κ_l of bulk FeSb₃ we calculated here. According to our result, the maximum l_{ph} is less than 600 nm. The sample size above this value is needed to safely avoid surface and grain boundary scatterings. Therefore the experimentally synthesized FeSb₃ films with the thicknesses of 1.0-1.5 μm [6] may be directly applied to measure the intrinsic κ_l and verify our theoretical prediction.**

TABLE S1. Optimized structure parameters by total energy minimization for FeSb_3 , CoSb_3 , $\text{LaFe}_4\text{Sb}_{12}$ and $\text{CeFe}_4\text{Sb}_{12}$, compared with available experimental data [9–11].

		Lattice parameter Fractional coordinates		
		a	x	y
FeSb₃	Theory	8.968	0.329	0.161
	Exp ⁹	9.154	0.334	0.158
CoSb₃	Theory	8.918	0.332	0.160
	Exp ¹⁰	9.0345		
LaFe₄Sb₁₂	Theory	8.985	0.335	0.164
	Exp ¹¹	9.148		
CeFe₄Sb₁₂	Theory	8.957	0.333	0.164
	Exp ¹¹	9.140		

-
- [1] W. Li, J. Carrete, N. A. Katcho, and N. Mingo, *Comput. Phys.* **185**, 1747 (2014).
 - [2] D. A. Broido, M. Malorny, G. Birner, N. Mingo, and D. A. Stewart, *Appl. Phys. Lett.* **91**, 231922 (2007).
 - [3] A. Ward, D. A. Broido, D. A. Stewart, and G. Deinzer, *Phys. Rev. B* **80**, 125203 (2009).
 - [4] W. Li, L. Lindsay, D. A. Broido, D. A. Stewart, and N. Mingo, *Phys. Rev. B* **86**, 174307 (2012).
 - [5] W. Li and N. Mingo, *Phys. Rev. B* **89**, 184304 (2014).
 - [6] A. Mochel, I. Sergueev, N. Nguyen, G. J. Long, F. Grandjean, D. C. Johnson, and R. P. Hermann, *Phys. Rev. B* **84**, 064302 (2011).
 - [7] W. Schnelle, A. Leithe-Jasper, H. Rosner, R. Cardoso-Gil, R. Gumeniuk, D. Trots, J. A. Mydosh, and Y. Grin, *Phys. Rev. B* **77**, 094421 (2008).
 - [8] M. M. Koza, M. Boehm, E. Sischka, W. Schnelle, H. Mutka, and A. Leithe-Jasper, *Phys. Rev. B* **91**, 014305 (2015).
 - [9] M. V. Daniel, L. Hammerschmidt, C. Schmidt, F. Timmermann, J. Franke, N. Johrmann, M. Hietschold, D. C. Johnson, B. Paulus, and M. Albrecht, *Phys. Rev. B* **91**, 085410 (2015).
 - [10] T. Caillat, A. Borschchevsky, and J. Fleurial, *J. Appl. Phys.* **80**, 4442 (1996).
 - [11] P. F. Qiu, J. Yang, R. H. Liu, X. Shi, X. Y. Huang, G. J. Snyder, W. Zhang, and L. D. Chen, *J. Appl. Phys.* **109**, 063713 (2011).